Progress In Electromagnetics Research B, Vol. 101, 45–61, 2023

Experimental Investigation of Novel Frock-Shaped Miniaturized 4×4 UWB MIMO Antenna Using Characteristic Mode Analysis

Ankireddy Chandra Suresh* **and Thatiparthi Sreenivasulu Reddy**

Abstract—In this paper, a novel frock-shaped four-port MIMO antenna is designed, and experimental results are verified for UWB applications. The four elements are placed orthogonal to each other to reduce mutual coupling. The proposed novel-shaped antenna is derived from a circular patch antenna. A series of modifications were made on a circular patch antenna to get the desired single, novel-shaped radiator. Inserting decoupling stubs in the plus form between MIMO elements lessened mutual coupling. The entire design procedure for the proposed four-port antenna was carried out by characteristic Mode Analysis. The proposed model is printed on an FR-4 substrate with dimensions of $40 \times 40 \times 1.6\,\text{mm}^3$. This novel 4-port antenna is well-operated in the UWB range from 2.8 GHz to 11.4 GHz and has a bandwidth of 8.6 GHz. The novelly shaped radiators with good decoupling stubs produce a high impedance bandwidth of 121.8%, radiation efficiency of 91%, high isolation of 26 dB, and gain of 6 dB in the operating band. The diversity parameters are the enveloped correlation coefficient (ECC) of less than 0.0011, diversity gain (DG) very near 10 dB, the capacity channel loss of 0.28 bp/s/Hz, and the mean effective gain of -3.1 dB. The experimental results of the antenna were verified with simulated ones, and there was good agreement between the fabricated and simulated results.

1. INTRODUCTION

The high data rates offered by ultra-wideband (UWB) Technology is an interesting feature in radio frequency (RF) communication. The unlicensed wireless band (UWB) spectrum, which ranges from 3.1 GHz to 10.6 GHz, was made available by the Federal Communications Commission (FCC) in 2002 [1]. internet of things (IoT) applications require high data rates as their utilization increases. The standard wireless communication system does not support high bandwidth and data rates. The novel UWB technology provides high data rates. As a result, the researchers prefer to design antennas in UWB [2]. The continuous development of antenna prototypes in short-range broad communication systems was satisfied by UWB technology. The main advantages of UWB are low hardware requirements and high data rates. However, because of its short range and low-density power, UWB suffers from multipath mitigation and fading. multiple-input multiple-output (MIMO) systems, which have the advantage of increasing spatial-multiplexing-gain and thus increasing spectral efficiency, were the best solution for UWB [3]. MIMO reduces the fading problem encountered by UWB. The combination of UWB-MIMO technologies can be used for video and media file transfer. The UWB-MIMO method permits investigators to develop antennas in small spaces. However, the compactness of the antennas is a challenge for designers when designing UWB-MIMO antennas [4]. MIMO systems allow their elements to be placed in a small area, which increases mutual coupling, and further intends to decrease the efficiency and reliability of wireless communication. This is a major issue while designing MIMO antennas for 5G and 6G communications [5]. Various decoupling methods are available to reduce mutual coupling and

Received 19 April 2023, Accepted 14 June 2023, Scheduled 3 July 2023
* Corresponding author: Ankireddy Chandra Suresh (archandu.suresh@gmail.com).
The authors are with the Department of Electronics and Communication Engineering, SVUCE, SV University, Tirupathi, A.P, India.

enhance the isolation between the MIMO elements like placing meta metals, stubs, neutralization lines, electromagnetic band gaps, and defected ground structures [6–20].

4×4 orthogonally placed MIMO antennas with a dimension of $80 \times 80 \times 1.6\,\text{mm}^3$ were printed on FR-4 material to produce the isolation 26 dB using a common ground plane [7]. Two circular monopoles were placed symmetrically and achieved more isolation greater than 31 dB in the entire UWB range. In MIMO, mutual coupling between two antenna elements can be canceled by properly adding an indirect coupling path [8]. With the help of metamaterials, a MIMO antenna along with antenna cutting, partial ground plane, and continuous shape modification has contributed to the isolation of more than 19 dB in the UWB range [9]. A U-shaped stub is placed between 4×4 MIMO antennas to investigate mutual coupling. This stub produces 20 dB isolation and diversity parameters that are within acceptable limits [10]. To improve impedance bandwidth, very thin slots are inserted in a 2×2 rectangular MIMO antenna. To improve isolation, parasitic elements were placed in a MIMO system and achieved 20 dB isolation [11]. Four pentagon-shaped radiators are orthogonally placed, and each radiator is inserted with a small slot, and parasitic elements in plus shape were placed on the ground to achieve good isolation around 20 dB [12, 13]. In a 2×2 UWB-MIMO antenna, the combination of rectangular and Z-shaped slots, as well as an inverted T-shaped slot near the ground plane, increased the isolation by more than 24.5 dB [14]. In a 2×2 MIMO antenna ground plane is flawed by two I-shaped slots located beneath the radiation elements. Each pair of radiation elements is 180° out of phase, so radiation interference was canceled, increasing isolation by more than 21 dB [15]. The proposed MIMO antenna achieved a high channel capacity of 1 bp/s/Hz using sophisticated design approaches such as channel simulations and optimized patterns [16]. In 4×4 UWB-MIMO, the mutual coupling between any two antenna elements should be less than -15 dB. For that cognitive radio technology was used. By connecting all ground planes in the MIMO, the mutual coupling is reduced. As a result, isolation increased to 19 dB [17]. The MIMO consists of two rectangular-shaped radiators placed on the same material. Each radiator cutting at the end of the patch achieved good isolation. Further isolation is achieved by inserting rectangular stubs between the elements, resulting in 25 dB isolation [18]. A small four-element UWB-MIMO antenna consists of two printed circuit boards (PCBs), with each one of dimensions $50 \times 25\,\text{mm}^2$. In UWB (2–12 GHz), a partial ground plane with an LC filter produces bandwidth up to 10 GHz and isolation greater than 17 dB [19]. The MIMO configuration consists of two antenna elements with dimensions of $100 \times 50 \times 0.8\,\text{mm}^3$, and operating bands 4.04 GHz to 5.48 GHz were achieved by using extreme edges of the substrate. Placing a metasurface-based isolator between MIMO elements achieved more than 23 dB of isolation [20]. The variable band gap center frequency and dual band gap stacked electromagnetic band gap (VBS-EBG) were used in the MIMO antenna to achieve isolation more than 16.16 dB [21]. The various decoupling networks are used to enhance the isolation in UWB MIMO antennas [22–24].

Mutual coupling increases as the number of radiators increases. If any of the methods listed above are used to reduce mutual coupling, it affects other parameters of the MIMO. For example, increasing isolation among the elements in MIMO reduces radiation efficiency and increases the envelop correlation coefficient. As the antenna designers did not use a systematic approach, good isolation in MIMO has an impact on the diversity parameters and radiation characteristics. The antenna designers used a trial-and-error method to achieve good isolation, which influences other MIMO parameters and is a time-consuming process. The requirements of reliable wireless communication are met through Characteristic Mode Analysis (CMA). CMA allows the antenna designers to analyze the antenna structures in physical insight. The use of CMA allows to get good diversity parameters and radiation parameters. With the aid of CMA, a unique 4×4 UWB MIMO antenna is created. The prerequisites for envelope correlation coefficient (ECC), diversity gain (DG), channel capacity loss (CCL), and mean effective gain (MEG) were met with this proposed antenna design.

2. DESIGN OF THE PROPOSED 4×4 UWB-MIMO ANTENNA

The proposed 4×4 frock-shaped antenna has dimensions of $40 \times 40 \times 1.6\,\text{mm}^3$ on a printed FR-4 substrate and $\tan\delta = 0.002$. The four radiators are frock-shaped and arranged orthogonally to each other to create space diversity on a 1.6 mm wide FR-4 substrate. The series of modifications on the circular patch radiator results in frock shaped radiators. The spacing between the two radiators is

Table 1. Specifications of frock shaped antenna.

Parameter	Value	Parameter	Value	Parameter	Value	Parameter	Value
Ws	40 mm	WL	40 mm	Wh	1.6 mm	Hp	0.0035 mm
$r1$	5 mm	$r2$	1.5 mm	$r3$	3 mm	$r4$	2 mm
$r5$	1.5 mm	$r6$	1.75 mm	$r7$	2.2 mm	$L2$	4.5 mm
$r9$	4.4 mm	$d2$	3 mm	Wf	1.5 mm	$W1$	2.8 mm
$L1$	6 mm	$W2$	8.7 mm	Lf	7.3 mm	$L3$	11 mm
$G1$	2.65 mm	$W3$	3 mm				

11 mm. The antenna's ground plane is designed with a defective ground structure and a plus-shaped stub to improve isolation. The optimized parameter values are depicted in Table 1.

2.1. Design Procedure of Single Frock Shaped Antenna

The frock-shaped single radiator is made up of a series of modifications in a circular patch antenna. A circular patch is designed with a radius of 5 mm on an FR-4 substrate width of 1.6 mm. A feed is added to the circular patch with the the width of 1.5 mm and length of 7.3 mm. A circle of radius 1.5 mm was removed from the circular radiator, and the resultant radiator is shown in Fig. 1(a). Using CST 2018, its characteristic modes are analyzed in a multi-layer solver or integral solver. For the aforementioned radiator, ten Characteristic Modes (CMs) were generated. Only one of the ten modes, Mode CM1, is practical and resonates at 5.6 GHz. The modal significances of the radiator shown in Fig. 1(a) are depicted in Fig. 2(a), and the characteristic currents of CM1 at 5.6 GHz are depicted in Fig. 3(a).

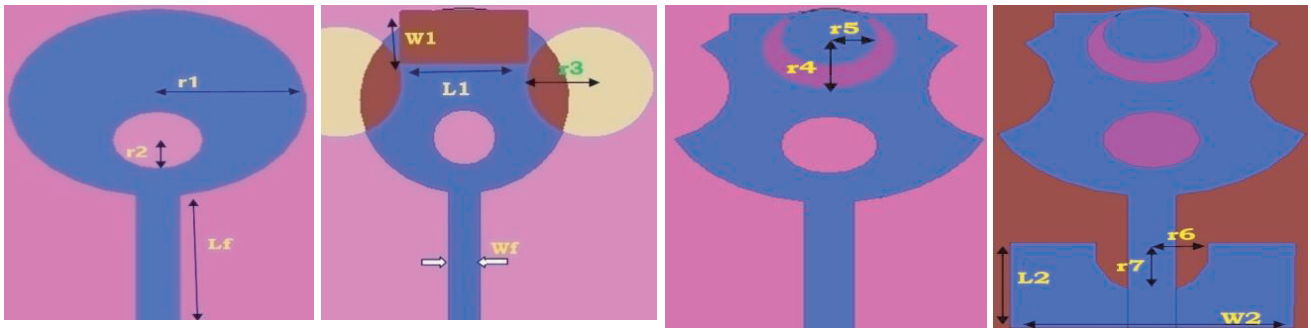

(a) (b) (c) (d)

Figure 1. Evaluation steps of single Frock shaped antenna.

A circular patch with a radius of 3 mm, which is centered at a distance of 1 mm from the substrate edge, and a height of 13 mm is removed from the circular radiator. The same is applied on another side of the radiator. A rectangular brick with dimensions of 2.8 mm width and 6 mm length is placed at a height of 14 mm from the lower edge of the circular radiator and depicted in Fig. 1(b). CMs of the antenna shown in Fig. 1(b) are analyzed and generated 10CMs. Out of them, 2 modes have resonant frequencies at 4.1 GHz and 11 GHz. But CMs at 11 GHz are not effective because it is beyond the UWB range. The corresponding modal significances of the antenna shown in Fig. 1(b) are depicted in Fig. 2(b), and the characteristics of currents at 4.1 GHz are depicted in Fig. 3(b). The operating characteristic modes are increased by making the changes in the radiator shown in Fig. 1(b). A circular patch with a radius of 2 mm at a height of 15 mm from the lower edge of the radiator is removed from the circular radiator. A 1.5 mm radius circular patch at a height of 15.6 mm from the lower edge of the radiator is added to the circular radiator, and the resultant radiator is shown in Fig. 1(c). Now the radiator's characteristic modes are examined as shown in Fig. 1(c). Ten CMs are generated in total,

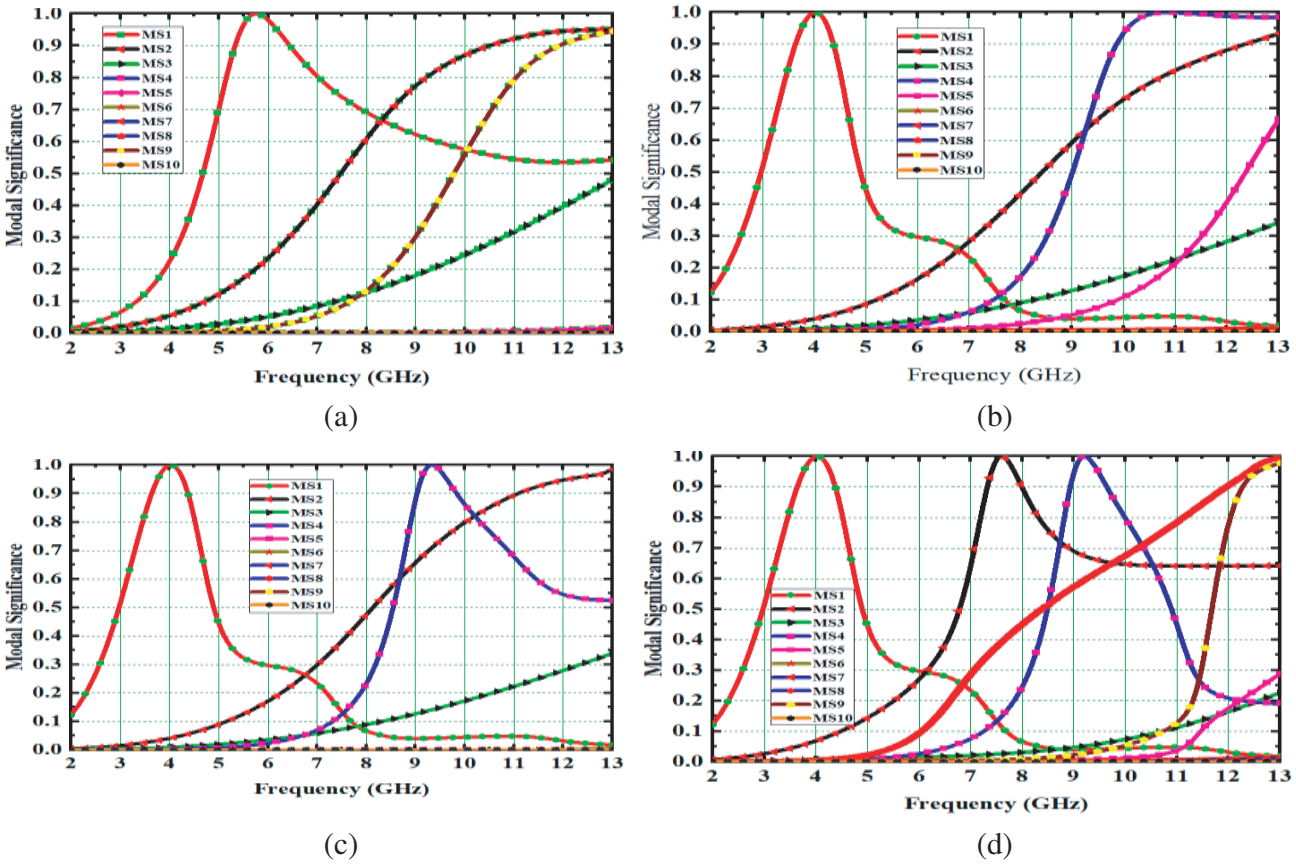

Figure 2. Modal significances of single Frock shaped antenna.

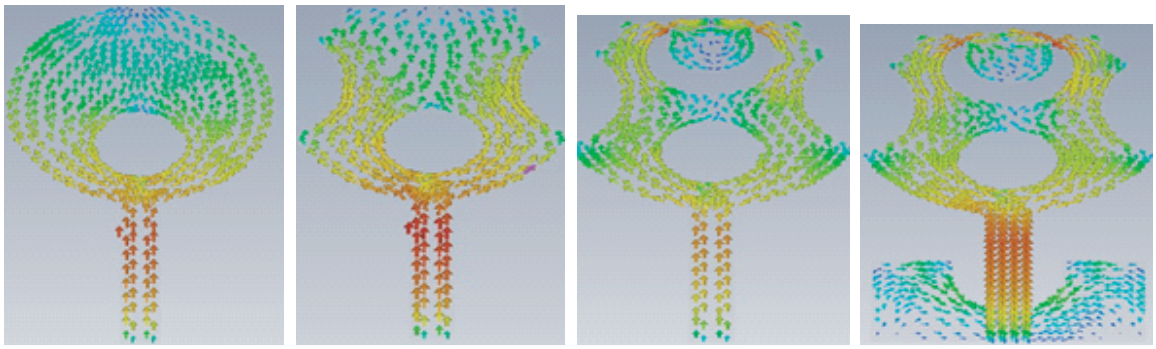

Figure 3. Characteristic current distributions of CM1 single Frock shaped antenna at 4.1 GHz in evolution process.

two of which are useful and resonate at 4.1 GHz (CM1) and 8.6 GHz (CM7), both of which are in the UWB range. The modal significances of the antenna shown in Fig. 1(c) are depicted in Fig. 2(c) and the characteristic current distributions at CM1 depicted in Fig. 3(c).

A rectangular conducting brick with dimensions of 8.7 mm in width and 4.5 mm in length is placed on the ground plane from the substrate's lower edge. An elliptical shape at a height of 4 mm from the lower edge of the substrate on the ground plane with a horizontal radius of 1.75 mm and a vertical radius of 2.2 mm is removed from the rectangular brick. The resultant frock-shaped single shape radiator is

shown in Fig. 1(d). 10 distinct modes are created for the radiator depicted in Fig. 1(d). Three of the ten modes are in the UWB range: CM1 (4.1 GHz), CM2 (7.6 GHz), and CM4 (9.1 GHz). CM1 is the dominant mode among these three modes because this mode is available in the evolution process of the single frock-shaped antenna. The corresponding CMs of the antenna shown in Fig. 1(d) are depicted in Fig. 2(d), and the CM's current distributions of CM1 at 4.1 GHz are depicted in Fig. 3(d).

3. SIGNIFICANCE OF CM THEORY

The single frock-shaped antenna designed using CMA employs a step-by-step design procedure. The CMA methodology is used to analyze the currents and electromagnetic fields generated by perfect electric conducting bodies of any shape or structure. Without the need for any excitation source, CMA understands the physical phenomena of radiators. The CMA is used to examine surface currents, characteristic mode currents, and the resonating frequency of a particular characteristic mode. Each characteristic mode has three properties i) Modal significance ii) Characteristic angle, iii) Eigenvalue. The Equations below express the characteristic current densities and electric fields (E_n) for any shape of conducting bodies of antennas.

$$\vec{J} = \sum_{n}^{N} \frac{\vec{J_n}\vec{E^i}}{1 + j\lambda_n}\vec{J_n} = \sum_{n}^{N} a_n \vec{J_n} \tag{1}$$

Here a_n is the common coefficient, and J_n is the characteristic current of the nth mode. The common coefficient is expressed as

$$a_n = \frac{(E^i_{\tan}(r))J_n}{1 + \lambda_n} \tag{2}$$

Here $E^i_{\tan}$ is the electric field. The Modal Significance (MS) is expressed as the normalized amplitude of current in CM where λ_n is equal to 0. The frequency at which MS = 1 is called the resonant frequency of the Characteristic mode. The characteristic angle (α_n) is represented in Equation (4)

$$MS_n = \frac{1}{1 + \lambda_n} \tag{3}$$

$$\alpha_n = 180^0 - \tan^{-1}(\lambda_n) \tag{4}$$

When λ_n is 0, α_n becomes 180°. For any mode, when α_n approaches 180°, those modes radiate effectively at their corresponding resonant frequencies, otherwise, store energy that is close to 90° or 270°.

4. DESIGN OF THE FROCK SHAPED 4×4 UWB-MIMO ANTENNA

The four frock-shaped radiators are printed on an FR-4 substrate with dimensions of $40 \times 40 \times 1.6\,\text{mm}^3$ with $\tan\delta = 0.002$ and $\varepsilon_r = 4.3$. The design process for a single frock-shaped radiator is shown in Fig. 1 and is described above. Now the antenna shown in Fig. 1(d) is placed orthogonally at a distance of 2.5 mm from each corner of the ground plane, and its top conducting radiators are separated by 11 mm and depicted in Fig. 4. The S_{11} of a single frock-shaped radiator is analyzed by increasing the above-said block L2's length from 4 mm to 5 mm. The respective S-parameters are evidenced in Fig. 5(a). The 4×4 frock-shaped radiator was created using this parametric study on L2 with $S_{11} < -10$ dB at 4.5 mm. The reflection coefficient of a 4×4 frock-shaped radiator is analyzed by increasing the ground block W2's width from 8.5 mm to 8.9 mm. The reflection coefficient is below 10 dB at a width of 8.7 mm. The parametric study on W2 is depicted in Fig. 5(b). The same process is repeated with different values of center circular patch radius ($r3$), upper circular patch with a diameter ($d2$) in the radiator, and the respective S_{11} shown in Fig. 5(c) and Fig. 5(d).

By placing a circular patch with a radius of ($r9$) 4.4 mm in the middle of the ground plane, the impedance bandwidth is enhanced more. Further isolation is enhanced by removing a circular patch in middle of the ground plane with a diameter ($d2$) of 3 mm. A 3 mm wide by 36 mm long plus-shaped decoupling stub is placed on the ground plane to improve the isolation of the proposed 4×4 frock-shaped antenna. The specifications of such 4×4 miniature frock-shaped antennas are displayed in Table 1.

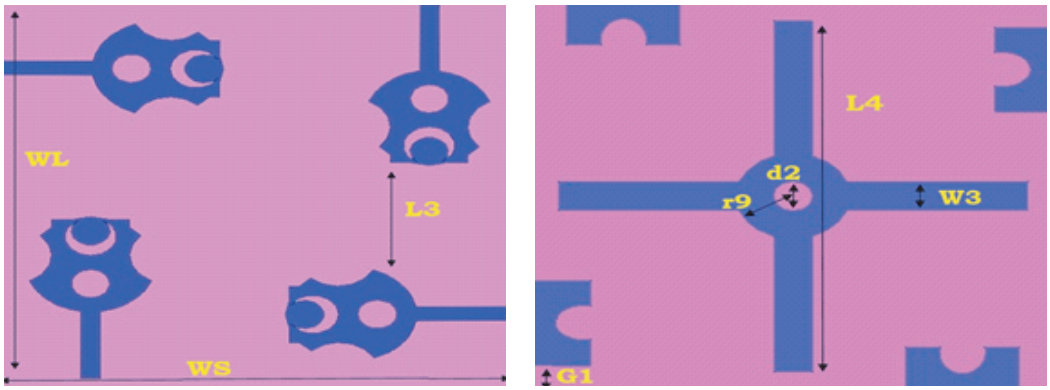

(a) (b)

Figure 4. Specifications for the proposed Frock-shaped 4×4 UWB-MIMO antenna. (a) Top view. (b) Bottom view.

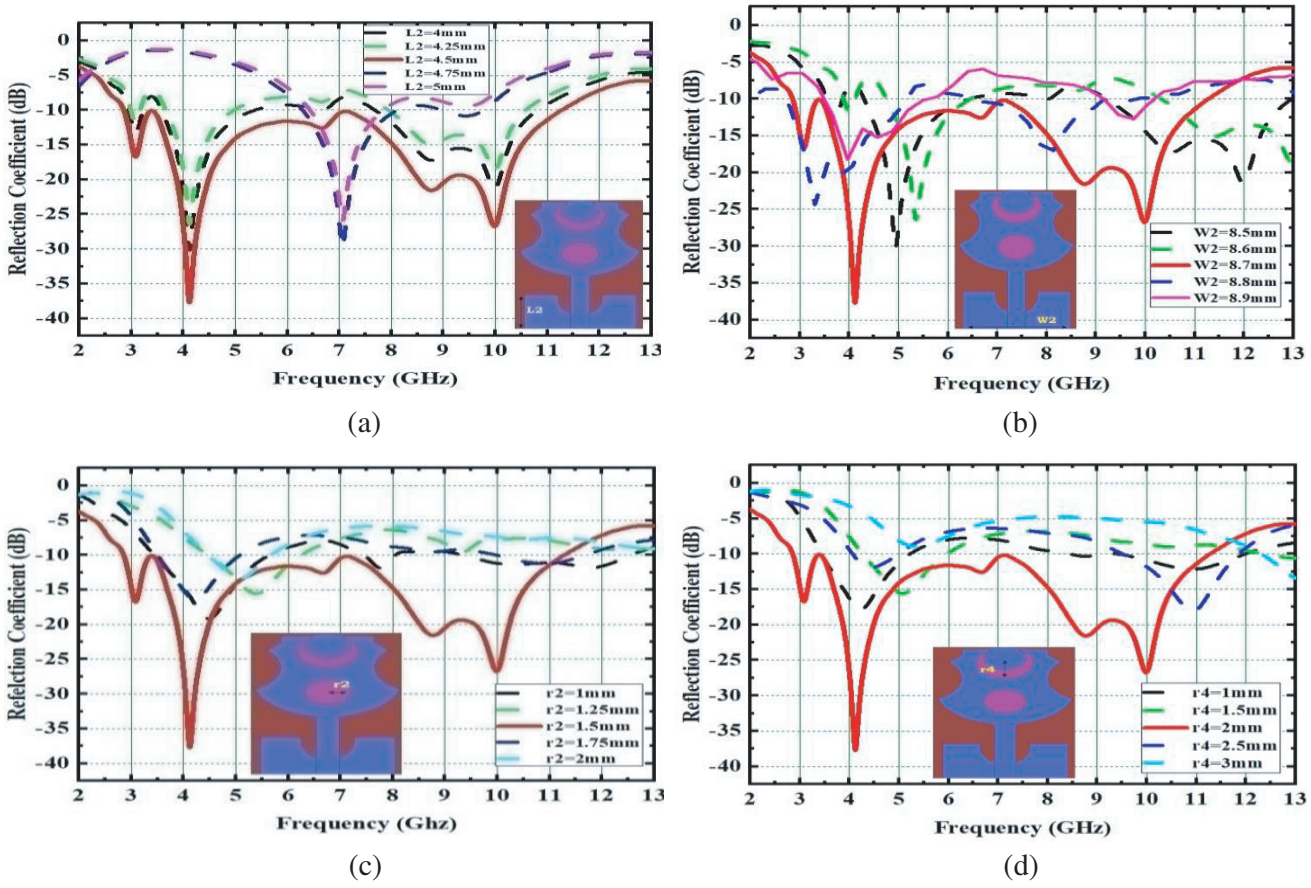

(a) (b)

(c) (d)

Figure 5. Parametric study of single frock radiator w.r.t (a) $L2$, (b) $W2$, (c) $r2$, (d) $r4$.

Four evaluation processes make up the proposed 4×4 frock-shaped antenna's overall design. These stages are antenna0 (A#0), antenna1 (A#1), antenna2 (A#2), and antenna3 (A#3). The key feature of the CMA is that antenna modal significances are examined without the need of any feed or excitation. The proposed antenna's diversity and radiation properties are enhanced as CMA employs step-by-step methodical design process. Fig. 6 shows the antenna design process in detail along with how it is evaluated.

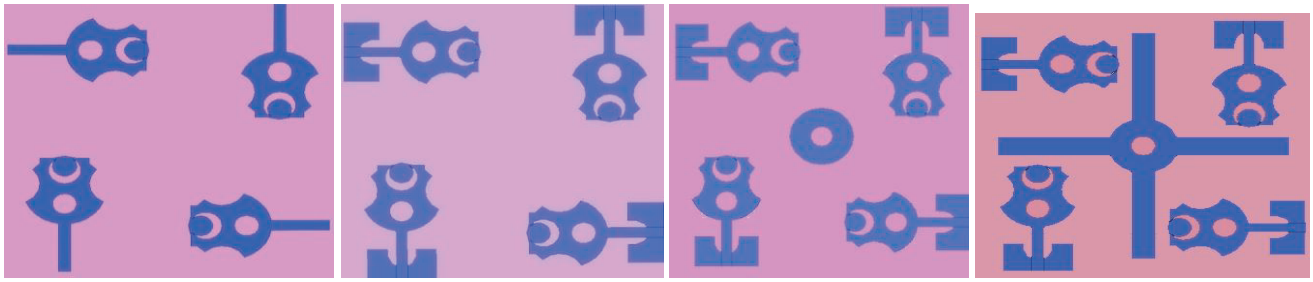

(a) (b) (c) (d)

Figure 6. Evolution process of 4×4 Frock shaped antenna. (a) A#0, (b) A#1, (c) A#2, (d) A#3.

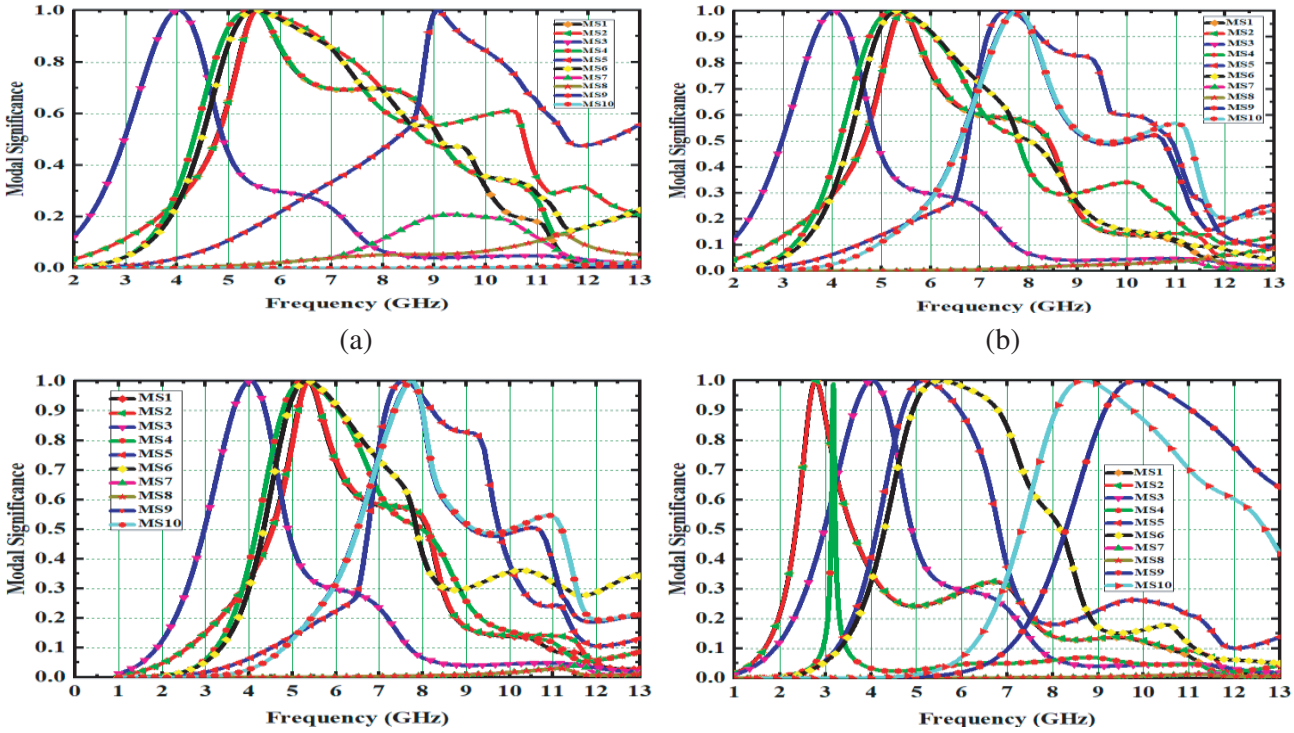

(a) (b)

(c) (d)

Figure 7. The modal significance of Frock-shaped antenna. (a) A#0, (b) A#1, (c) A#2, (d) A#3.

The radiator shown in Fig. 1(c) Antenna#0, i.e., A#0, is created by orthogonally arranging a frock-shaped antenna on FR-4 material, and its characteristic modes are evaluated. Antenna A#0 is evidenced in Fig. 6(a). Ten CMs in total are generated. However, only a few CMs are useful for adding bandwidth to UWB. The concentration of CM1, CM2, CM3, and CM4 occurs between 4 GHz and 5 GHz, and CM5 occurs at 9 GHz [25]. There are no bandwidth contributions from the remaining modes. No CMs are scattered at low or high frequencies in antenna A#0. The respective modal significances are evidenced in Fig. 7(a). A#0 will be excited with the source, and the S-parameters will be examined. The corresponding S-parameters are depicted in Fig. 8(a). The antenna shown in Fig. 1(d) is arranged on a 4×4 setup to form antenna A#1. A#1 is analyzed and generates ten CMs. Some of them contribute bandwidth in the UWB range. At 5.6 GHz, CM1, CM2, CM4, and CM6 are resonant. At 4.1 GHz, CM3 is resonant. At 7.5 GHz, CM5, CM9, and CM10 are resonant. CMs7 and CM8 do not provide any UWB bandwidth. All of the user modes in A#1 are concentrated only in the

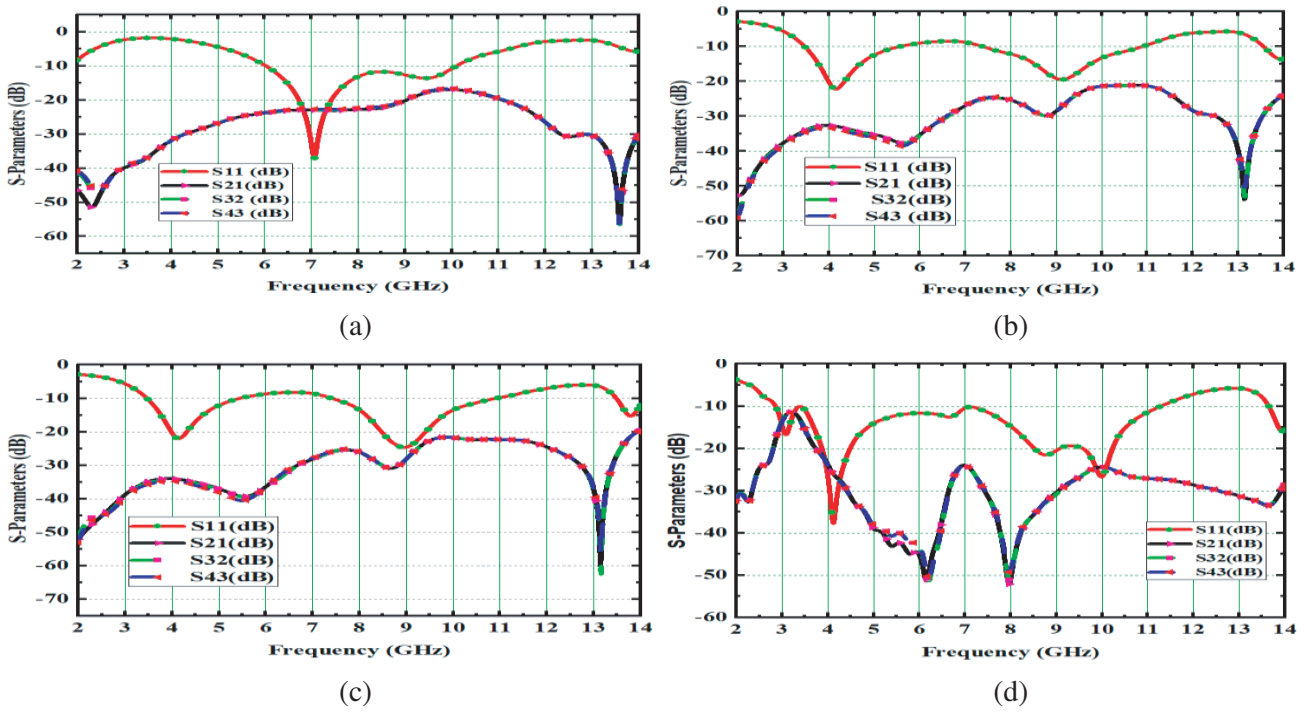

Figure 8. The S-parameter of Frock-shaped antenna. (a) A#0, (b) A#1, (c) A#2, (d) A#3.

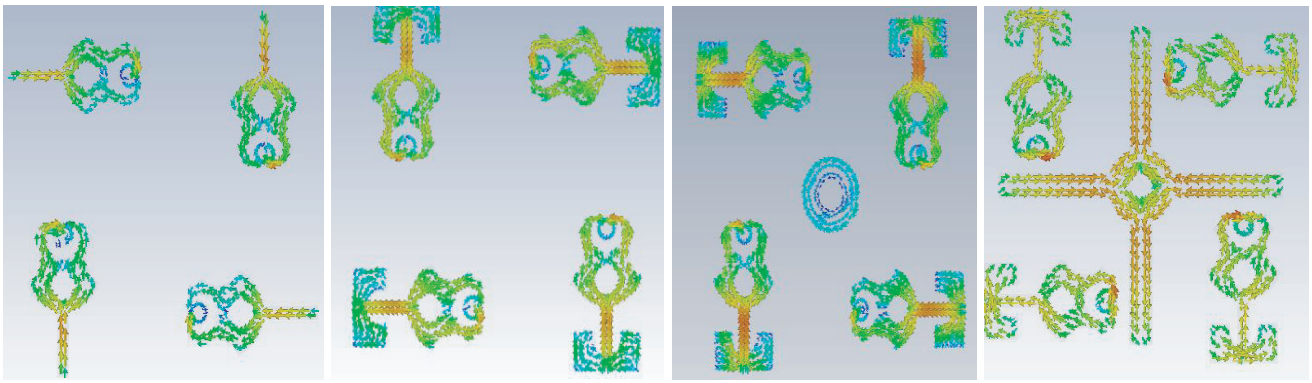

Figure 9. Fundamental characteristic mode current effect in the evolution of Frock-shaped antenna.

mid-band frequencies region according to this research. The corresponding modal significances of A#1 are evidenced in Fig. 7(b). The Fundamental Characteristic Mode Current effect in the evolution of frock-shaped antenna is evidenced in Fig. 9. The characteristic current distributions of A#1 at various frequencies are evidenced in Fig. 10. The appropriate stubs in between radiators are placed to increase the bandwidth and isolation in the low and high frequencies.

4.1. Impact of Plus Shaped Decoupling on Ground Plane

A circular patch with radius of ($r9$) 4.4 mm is added on the center of the ground plane in Antenna A#1. A circular patch with a diameter ($d2$) of 3 mm is removed from the above said circular patch. The resultant antenna is called A#2 and is depicted in Fig. 6(c). The A#2 characteristic modes are

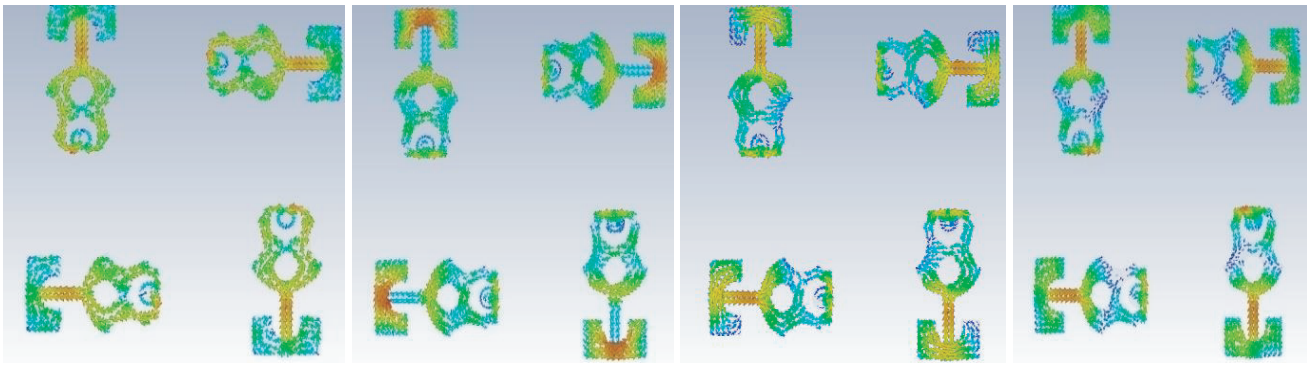

(a) (b) (c) (d)

Figure 10. Characteristic currents of CM3 in A#1 at (a) 4.1 GHz, (b) 6.6 GHz, (c) 8.7 GHz, and (d) 10 GHz.

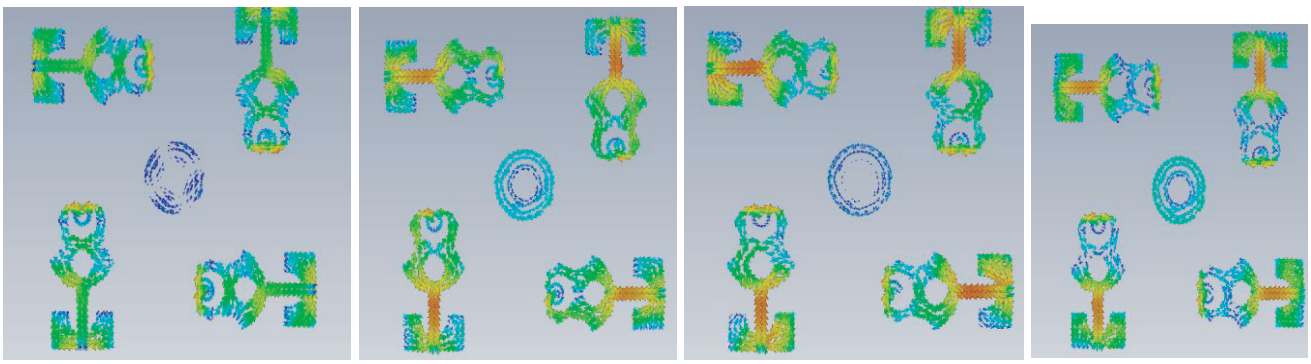

(a) (b) (c) (d)

Figure 11. Characteristic currents of CM3 in A#2 at (a) 4.1 GHz, (b) 6.6 GHz, (c) 8.7 GHz, and (d) 10 GHz.

examined. Ten CMs altogether are produced. Some of the ten modes contribute bandwidth in the UWB spectrum. CM1, CM2, CM4, CM5, and CM6 resonate at 5.6 GHz, as CM9 and CM10 resonate at 7.8 GHz. At 4.1 GHz, CM3 is resonant. In UWB, CM7 and CM8 do not contribute any bandwidth. Based on the above data, all modes are not scattered throughout the whole UWB region [26]. At the mid-band frequency, all CMs are concentrated. This A#2 is good at mid-band frequencies only. The corresponding modal significances of A#2 are depicted in Fig. 7(c). The characteristic mode current distributions of A#2 at various frequencies are evidenced in Fig. 11. A plus-shaped stub of 36 mm long and 3 mm wide is added, starting from the center of antenna A#2's ground plane. The resultant is called A#3 antenna and depicted in Fig. 6(d). CM theory is utilized to analyze A#3 characteristic modes. There are 10 distinct characteristic modes in all. A total of 10 characteristic modes are scattered in UWB to increase bandwidth and isolation. At 2.8 GHz, 3 GHz, and 3.2 GHz, CM1, CM2, and CM4 are resonant in the low-frequency region. CM3 is resonant at 4.1 GHz. CM5 and CM6 are concentrated at 5.6 GHz and 6.8 GHz. CM9 and CM10 resonate at a high-frequency range of 10 GHz and 8.9 GHz. The remaining modes CM7 and CM8 do not contribute any bandwidth in the UWB range. The characteristic mode current distributions of A#3 at various frequencies are evidenced in Fig. 12. The current densities of A#3 at different frequencies are evidenced in Fig. 13. According to this analysis, some characteristic modes resonate at mid-band frequencies (4 GHz–8 GHz); some modes resonate at high-frequency regions (8 GHz–10 GHz); and some CMs resonate in low-frequency regions (2 GHz–4 GHz). It means that this model Antenna A#3 contribute good isolation and impedance bandwidth in the UWB region [27]. The respective modal significances are evidenced in Fig. 7(d). Feed and excitation are applied to four

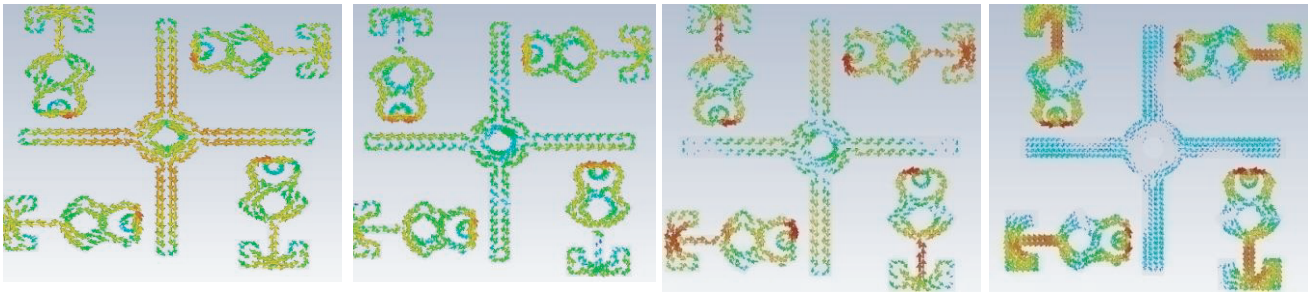

(a) (b) (c) (d)

Figure 12. Characteristic currents of CM3 in A#3 at (a) 4.1 GHz, (b) 6.6 GHz, (c) 8.7 GHz, and (d) 10 GHz.

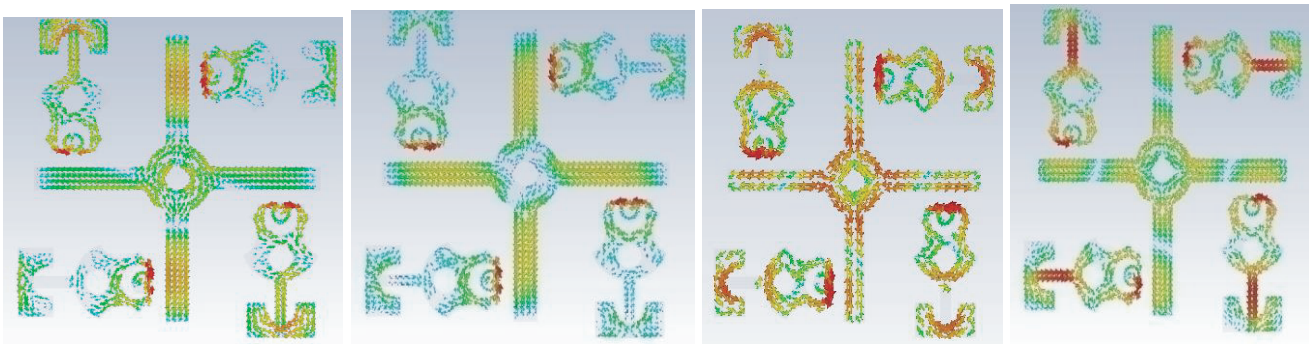

(a) (b) (c) (d)

Figure 13. Current densities in A#3 at (a) 4.1 GHz, (b) 6.6 GHz, (c) 8.7 GHz, and (d) 10 GHz.

antennas from A#0 to A#3. The respective resultant S-parameters are shown in Fig. 8, respectively [28]. The equivalent circuit diagram of proposed MIMO antenna is depicted in Fig. 14. A circular patch with a radius of $r2$ is removed from the single radiator to get S_{11} below -10 dB. Using a parametric study on $r2$ (from 1 mm to 2 mm), the best S_{11} is achieved at the radius of 1.5 mm. The frequency of operation of MIMO depends on the tank circuit which consists of $L3$, $C3$. When applying the parametric analysis on $r4$ (from 1 mm to 3 mm) the best frequency of operation at $r4$ equals 2 mm. Varying the $r4$ in turn varies the tank circuit values $L3$ and $C3$. Parametric analysis is applied on $L2$ and $W2$ which also shows the impact on $L3$ and $C3$. The best resonant mode is achieved at $L2 = 4.5$ mm and $W2 = 8.7$ mm.

5. EXPERIMENTAL INVESTIGATION OF 4×4 FROCK SHAPED UWB MIMO ANTENNA

High-end equipment is used to fabricate the planned 4×4 frock-shaped antenna, and its simulation and testing results are compared. There is a strong correlation between test findings and simulation outcomes. The S-parameters S_{11}, S_{21}, S_{32}, and S_{43} are measured using the N5247 Vector network analyzer. The fabricated antenna is depicted in Fig. 15. This antenna provides good isolation between the MIMO elements, greater than 26 dB, and good impedance bandwidth in 3.1 GHz to 10.6 GHz range. The comparison of the measured and simulated results of S_{11} are displayed in Fig. 16. The frock-shaped 4×4 antenna achieves the $S_{11} < -10$ dB in the entire UWB range. Fig. 17(a) depicts the isolation measured results, and Fig. 17(b) explains the anechoic chamber setup.

Using an anechoic chamber, the co-polarization and cross-polarization at 4.1 GHz, 8.6 GHz, and 10 GHz are measured and shown in Fig. 18. The radiation efficiency and gain are 91% and 6 dB, respectively [29] as depicted in Fig. 19.

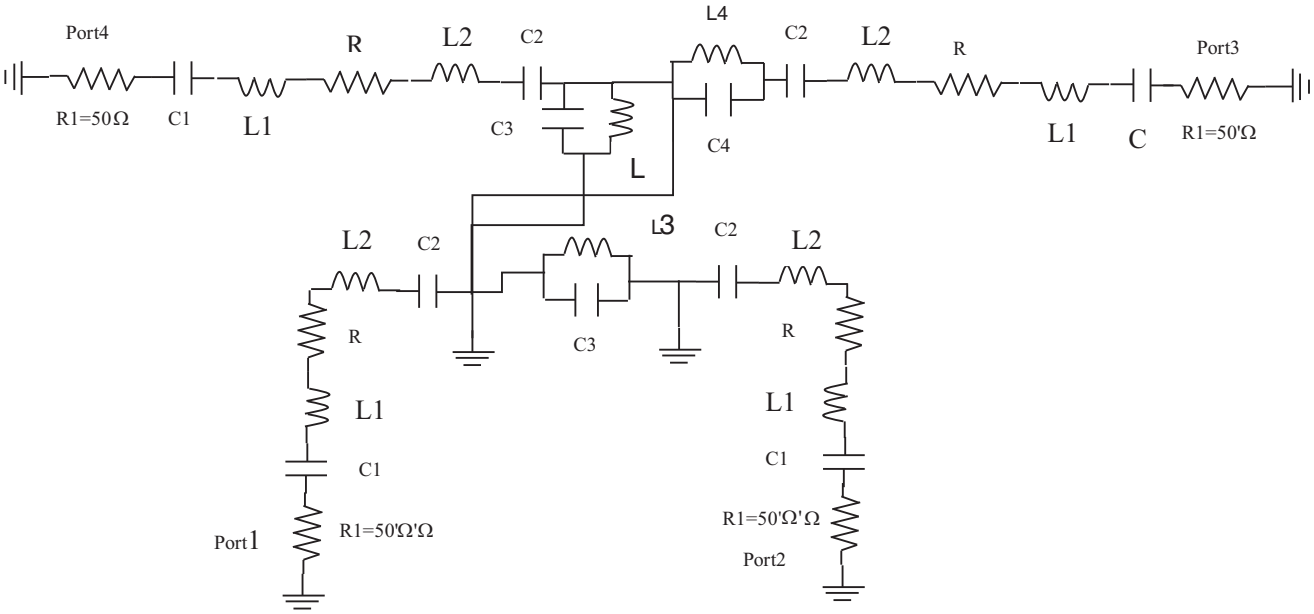

Figure 14. Frock shaped 4×4 UWB-MIMO antenna equivalent circuit diagram.

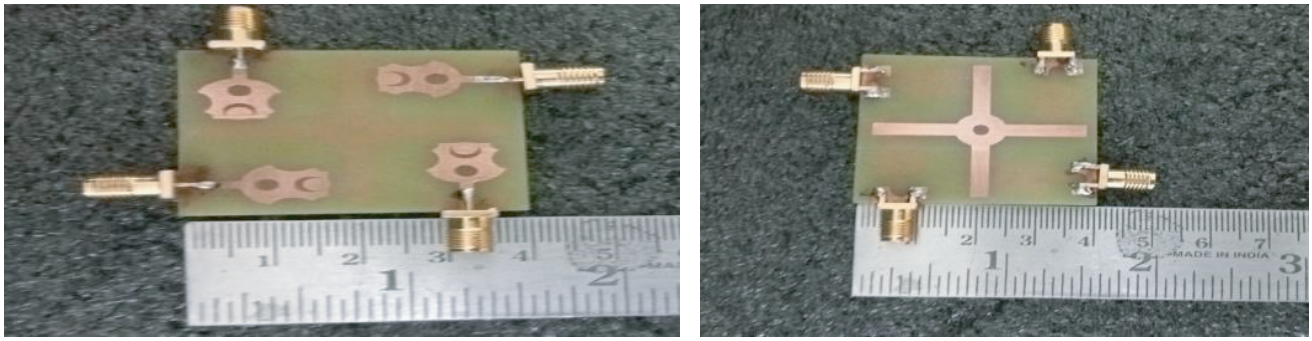

(a) (b)

Figure 15. Frock shaped 4×4 UWB-MIMO prototype. (a) Front view. (b) Back view.

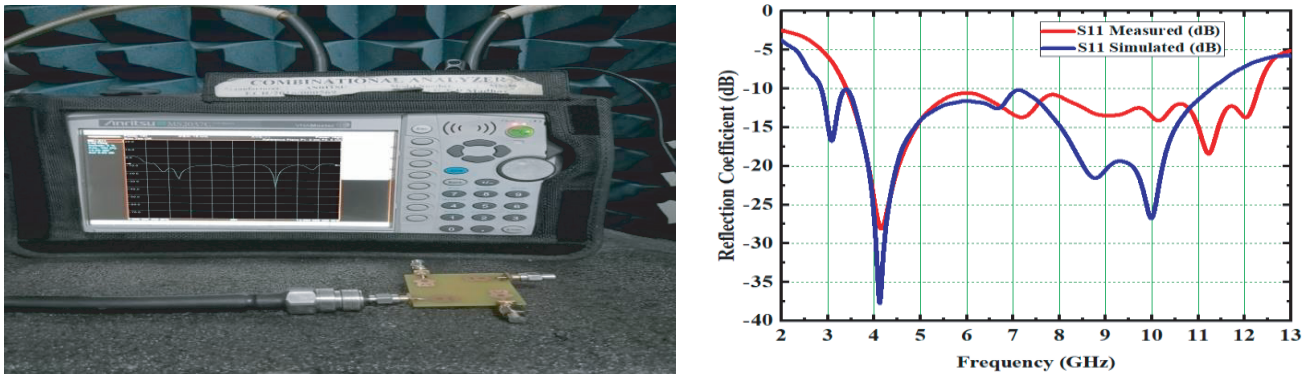

(a) (b)

Figure 16. (a) S_{11} measured, (b) S_{11} measured with simulated.

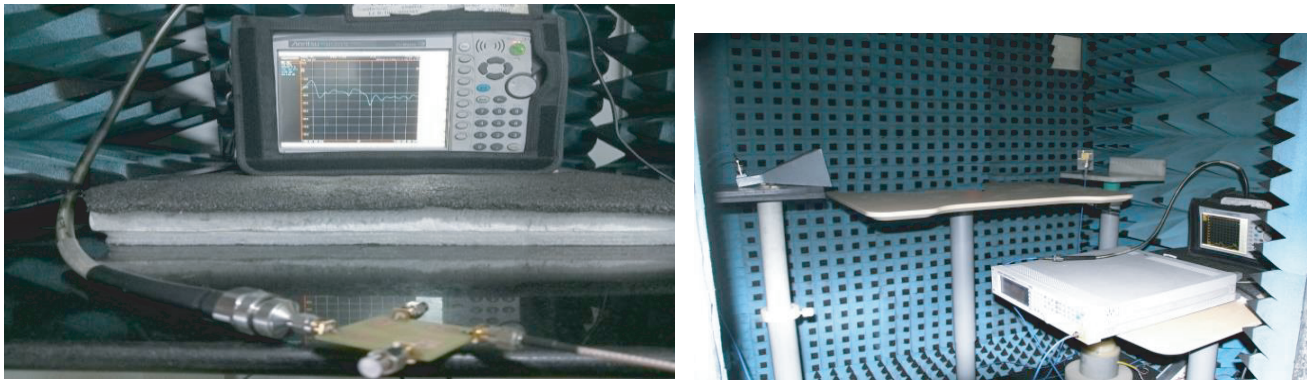

(a) (b)

Figure 17. (a) Isolation measurement. (b) Anechoic chamber setup.

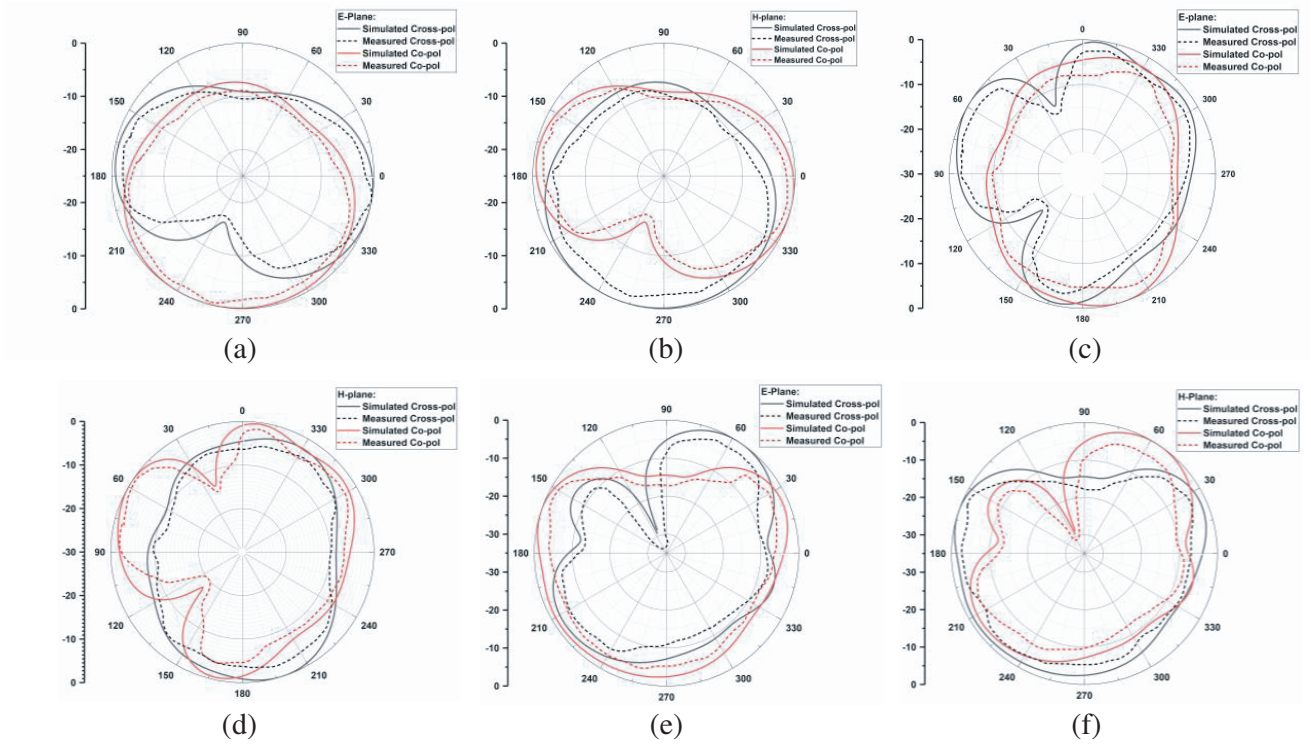

(a) (b) (c)

(d) (e) (f)

Figure 18. The frock shaped 4×4 antenna co-polarization and cross polarization of E-plane at (a) 4.1 GHz, (c) 8.6 GHz, (e) 10 GHz and H-plane at (b) 4.1 GHz, (d) 8.6 GHz, (f) 10 GHz.

The effective MIMO antenna has good diversity characteristics. Low mutual coupling is one of its properties that has an impact on MIMO performance. S-parameters or far-fields of a MIMO antenna are used to measure the envelope correlation coefficient (ECC). The ECC indicates, in a MIMO system, the interaction of one radiator with other radiators. ECCs must be below 0.5. The ECC is computed using S-parameters. Here S_{11} and S_{22} are return losses at their respective ports. S_{12} and S_{21} are isolation parameters between port 1 and port 2

$$\rho_{12} = \frac{\left|S_{11}^{*}S_{12} + S_{21}^{*}S_{22}\right|^{2}}{\left(1 - \left(|S_{11}|^{2} - |S_{21}|^{2}\right)\right)\left(1 - \left(|S_{22}|^{2} - |S_{12}|^{2}\right)\right)} \tag{5}$$

The ECC of the proposed antenna is less than 0.0011 and depicted in Fig. 20(b). ECC in MIMO

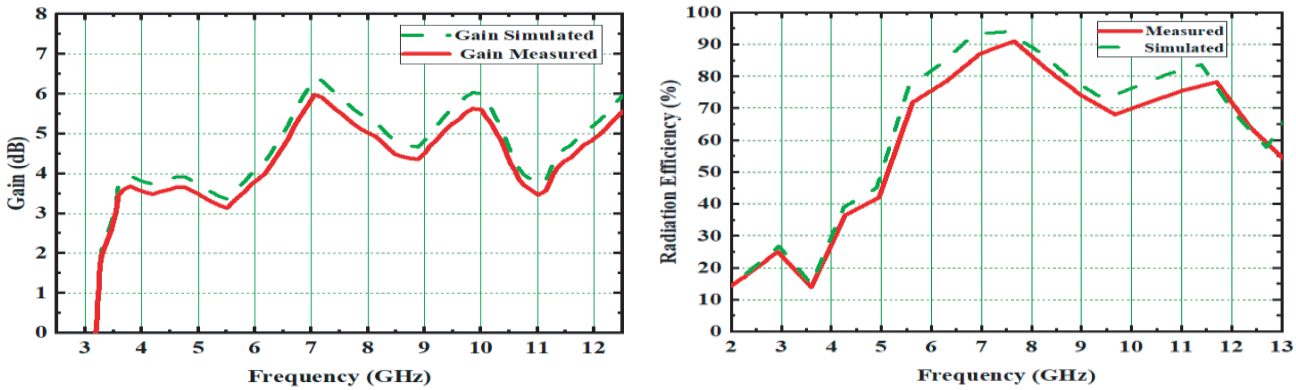

(a) (b)

Figure 19. (a) Gain simulated with tested, (b) radiation efficiency.

is calculated using Equation (5) because it contains two components. ECC is additionally calculated using [30] far fields whenever a MIMO system has more than two antenna elements.

$$\rho_e = \frac{\left|\int_0^{2\pi}\int_0^{\pi}\left(XPR\cdot E_{\theta 1}\cdot E_{\theta 2}^{*}P_{\theta}+E_{\Phi 1}E_{\Phi 2}^{*}\cdot P_{\Phi}\right)d\Omega\right|^2}{\int_0^{2\pi}\int_0^{\pi}\left(XPR\cdot E_{\theta 1}\cdot E_{\theta 1}^{*}P_{\theta}+E_{\Phi 1}E_{\Phi 1}^{*}\cdot P_{\Phi}\right)d\Omega X\int_0^{2\pi}\int_0^{\pi}\left(XPR\cdot E_{\theta 2}\cdot E_{\theta 2}^{*}P_{\theta}+E_{\Phi 2}E_{\Phi 2}^{*}\cdot P_{\Phi}\right)d\Omega} \tag{6}$$

where XPR is called cross-polarization ratio. The average signal-to-noise ratio of all MIMO signals transmitted by a single antenna and received via various pathways at the receiver end is measured called the diversity gain. The proposed antenna achieves > 9.998 dB diversity gain as depicted in Fig. 20(a). The diversity gain is also derived from the ECC [31].

$$DG = 10\sqrt{1-ECC^2} \tag{7}$$

$$DG = \left[\left(\frac{\gamma_c}{SNR_c}-\frac{\gamma_1}{SNR_1}\right)_{P\left(\gamma_c<\frac{\gamma_s}{SNR}\right)}\right] \tag{8}$$

MEG is another crucial MIMO diversity metric. The term "mean effective gain" refers to the amount of power received by the MIMO diversity antenna relative to an isotropic antenna in fading conditions. The MEG of the proposed MIMO is -3.1 dB as evidenced in Fig. 21(a). The MEG is analyzed by

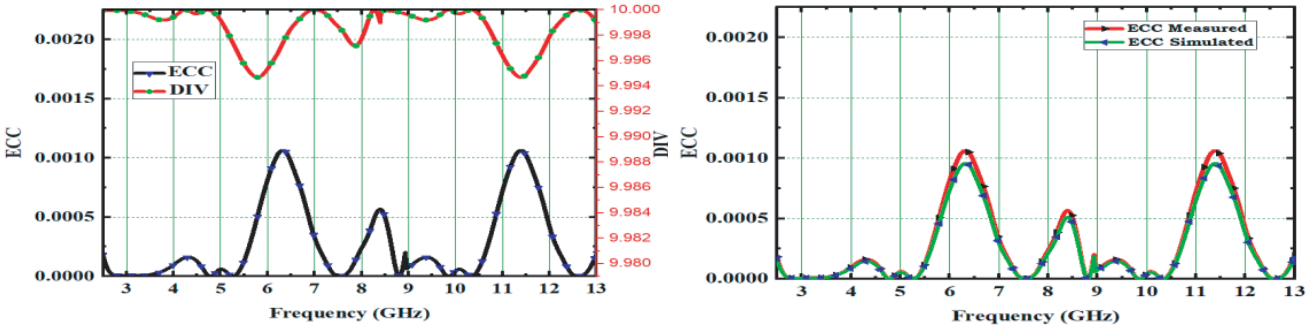

(a) (b)

Figure 20. (a) ECC with DG, (b) ECC.

Equation (9)

$$MEG_i = 0.5\left(1 - \sum_{j=1}^{k} |S_{ij}|^2\right) \tag{9}$$

CCL (channel capacity loss) is another key parameter of MIMO [32]. The CCL is a crucial matrix for assessing the impact of a MIMO antenna structure. The CCL must be less than 0.4 bits/s/Hz for a good MIMO system. Fig. 21(b) displays the measured as well as simulated values of CCL. In the UWB spectrum, the designed frock-shaped antenna attaines 0.28 bits/s/Hz.

The CCL is expressed as

$$CCL = -\log_2 \det\left(\psi^R\right) \tag{10}$$

$$\psi^R = \begin{bmatrix} \varrho_{11} & \varrho_{12} & \varrho_{13} & \varrho_{14} \\ \varrho_{21} & \varrho_{22} & \varrho_{23} & \varrho_{24} \\ \varrho_{31} & \varrho_{32} & \varrho_{33} & \varrho_{34} \\ \varrho_{41} & \varrho_{42} & \varrho_{43} & \varrho_{44} \end{bmatrix} \tag{11}$$

$$y_{ii} = \left(1 - |S_{ii}|^2 - |S_{ij}|^2\right) \quad \text{and} \quad y_{ij} = \left(S_{ii}^* S_{ij} + S_{ji}^* S_{ij}\right) \quad \text{for} I,\ j = 1 \text{ or } 2 \tag{12}$$

Table 2. Comparison of proposed model with existing models.

Ref.	Dimensions	Isolation Technique	Isolation (dB)	Gain (dB)	DG	ECC	Radiation Efficiency %	CCL
[28]	$40 \times 40 \times 1.6$	Swastik Shape stub	< -18	5.5		< 0.012	> 89	< 0.3
[29]	$40 \times 40 \times 1.6$	T-shaped decoupling stub	< -25	5.6	> 9.92	< 0.0045	> 90	< 0.39
[30]	$40 \times 40 \times 1.6$	DGS	< -26	4.9	> 9.92	< 0.0016	> 89	< 0.29
[31]	$93 \times 93 \times 1.6$	Fratcal with resistive load	< -20	5.4	> 9.8	< 0.003	82	< 0.4
[32]	$30 \times 30 \times 1.6$	MTS & DGS	< -17	6.2	> 9.9	< 0.001	87	< 0.1
[33]	40×40	Meta Surface	< -27	8.5	—	—	76	
[34]	$56 \times 68 \times 0.2$	Diamond Shaped slot	< -15	5.87	—	< 0.02	—	< 0.5
[35]	$80 \times 80 \times 1.6$	Split Ground	< -25	5.8	> 9.9	< 0.02	80	< 0.4
[36]	$48 \times 34 \times 1.6$	Neutralization lines	< -23	2.91	> 9.981	< 0.0039	79.8	< 0.29
[37]	$74 \times 74 \times 1.524$	Parasitic elements & slots	< -34	7.68	—	—	94	—
[38]	$36 \times 35 \times 1.6$	DGS	< -17	—	> 9.99	< 0.012	—	< 0.4
[39]	$40 \times 40 \times 1.6$	DGS	< -15	3.5	—	< 0.4	> 89	—
Prop.	$40 \times 40 \times 1.6$	Plus Shaped Stub	< -26	6	> 9.99	< 0.0011	> 90	< 0.28

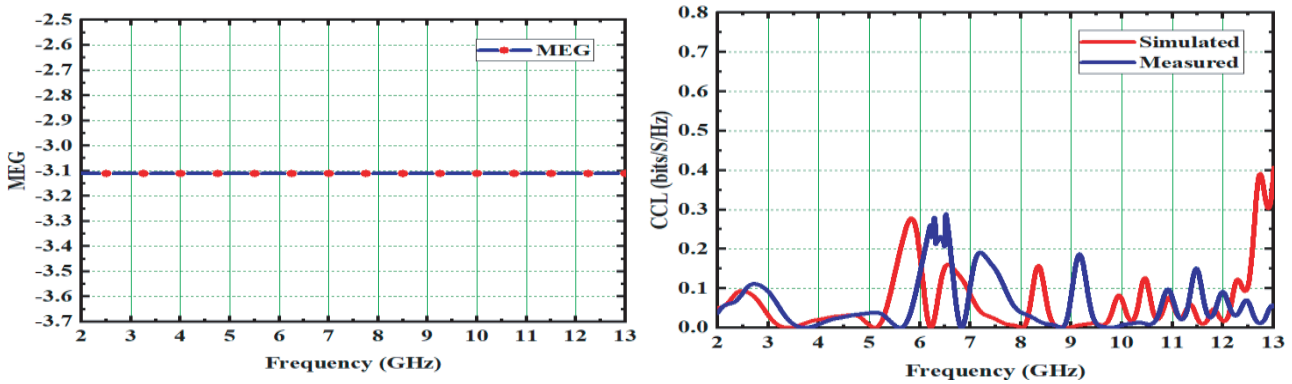

(a) (b)

Figure 21. (a) MEG. (b) CCL.

6. COMPARISONS WITH EXISTING MODELS

In terms of size, bandwidth, gain, and diversity factors like ECC, MEG, CCL, and radiation parameters, the proposed working model is compared to existing working models [28–39] in Table 2. Comparative analysis reveals that the suggested antenna with CMA methodological design improves the diversity metrics ECC, DG, and CCl across the whole UWB.

7. CONCLUSION

A 4×4 UWB-MIMO antenna in the shape of a frock that operates from 2.8 GHz to 11.4 GHz utilizing the CMA approach is proposed. Using CMA, the frock-shaped MIMO antenna achieves good radiation properties and diversity parameters. By inserting a plus-shaped stub between radiators oriented orthogonally to one another, the high isolation of more than 26 dB is achieved. With a gain of 6 dB, this plus-shaped stub offers a stable and consistent radiation pattern in the *E*- and *H*-planes. This antenna gets a large impedance bandwidth of 121.8% and a 91% radiation efficiency due to its innovative frock shape. According to the experimental examination, the ECC, DG, MEG, and CCL diversity characteristics of this antenna are 0.0011, 9.998, −3.1 dB, and 0.29 bits/s/Hz, respectively. The proposed antenna is suitable for UWB applications.

REFERENCES

1. Ellis, M. S., P. Arthur, A. R. Ahmed, J. J. Kponyo, B. Andoh-Mensah, and B. John, "Design and circuit analysis of a single and dual band-notched UWB antenna using vertical stubs embedded in feedline," *Heliyon*, Vol. 7, No. 12, e08554, 2021.
2. Kaiser, T., F. Zheng, and E. Dimitrov, "An overview of ultra-wide-band systems with MIMO," *Proc. IEEE*, Vol. 97, 285–312, 2009.
3. Sultan, K. S. and H. H. Abdullah, "Planar UWB MIMO-diversity antenna with dual notch characteristics," *Progress In Electromagnetics Research C*, Vol. 93, 119–129, 2019.
4. Kulkarni, J., A. Desai, and C. Y. D. Sim, "Wideband four-port MIMO antenna array with high isolation for future wireless systems," *AEU — International Journal of Electronics and Communications*, Vol. 128, 153507, 2021.
5. Parvathi, K. S. L. and S. R. Gupta, "Novel dual-band EBG structure to reduce mutual coupling of air gap based MIMO antenna for 5G application," *AEU — International Journal of Electronics and Communications*, Vol. 138, 153902, 2021.

6. Chithradevi, R. and B. S. Sreeja, "A compact UWB MIMO antenna with high isolation and low correlation for wireless applications," *2017 IEEE International Conference on Antenna Innovations & Modern Technologies for Ground, Aircraft and Satellite Applications (iAIM)*, Banglore, India, Nov. 24–26, 2017.
7. Rekha, V. S. D., P. Pardhasaradhi, B. T. P. Madhav, and Y. U. Devi, "Dual band notched orthogonal 4-element MIMO antenna with isolation for UWB applications," *IEEE Access*, Vol. 8, 145871–145880, 2020.
8. Radhi, A. H., R. Nilavalan, Y. Wang, H. S. Al-Raweshidy, A. A. Eltokhy, and N. Ab Aziz, "Mutual coupling reduction with a wideband planar coupling structure for UWB-MIMO antenna," *Int. J. Microwave Wireless Technol.*, Vol. 10, 1143–1154, 2018.
9. Urimubenshi, F., D. B. Konditi, J. de Dieu Iyakaremye, P. M. Mpele, and A. Munyaneza, "A novel approach for low mutual coupling and ultra-compact two port MIMO antenna development for UWB wireless application," *Heliyon*, Vol. 8, No. 3, e09057, 2022.
10. Hasan, M. N., S. Chu, and S. Bashir, "A DGS monopole antenna loaded with U-shape stub for UWB MIMO applications," *Microwave and Optical Technology Letters*, Vol. 61, No. 9, 2141–2149, 2019.
11. Kim-Thi, P., H. H. Tran, and T. T. Le, "Circularly polarized MIMO antenna utilizing parasitic elements for simultaneous improvements in isolation, bandwidth and gain," *AEU — International Journal of Electronics and Communications*, Vol. 135, 153727, 2021.
12. Nikam, B. V. and M. R. Jadhav, "A compact quad port band-notched MIMO antenna for Wi-Max applications with low mutual coupling," *Progress In Electromagnetics Research C*, Vol. 104, 53–67, 2020.
13. Luo, S., D. Wang, Y. Chen, E. Li, and C. Jiang, "A compact dual-port UWB-MIMO antenna with quadruple band-notched characteristics," *AEU — International Journal of Electronics and Communications*, Vol. 136, 153770, 2021.
14. Chattha, H. T., F. Latif, F. A. Tahir, M. U. Khan, X. Yang, "Small-sized UWB MIMO antenna with band rejection capability," *IEEE Access*, Vol. 7, 121816–121824, 2019.
15. Alibakhshikenari, M., B. S. Virdee, C. H. See, P. Shukla, S. M. Moghaddam, A. U. Zaman, and E. Limiti, "Dual-polarized highly folded bowtie antenna with slotted self-grounded structure for sub-6GHz 5G applications," *IEEE Transactions on Antennas and Propagation*, Vol. 70, No. 4, 3028–3033, 2021.
16. Kowalewski, J., J. Eisenbeis, M. Tingulstad, Z. Kollar, and T. Zwick, "Design method for capacity enhancement of pattern-reconfigurable MIMO vehicular antennas," *IEEE Antennas and Wireless Propagation Letters*, Vol. 18, No. 12, 2557–2561, 2019.
17. Thummaluru, S. R., M. Ameen, and R. K. Chaudhary, "Four-port MIMO cognitive radio system for midband 5G applications," *IEEE Transactions on Antennas and Propagation*, Vol. 67, No. 8, 5634–5645, 2019.
18. Haripriya, D., S. Venkatakiran, and A. Gokulachandar, "UWB-MIMO antenna of high isolation two elements with WLAN single band-notched behavior using roger material," *Materials Today: Proceedings*, Vol. 62, 1717–1721, 2022.
19. Khan, M. S., S. A. Naqvi, A. Iftikhar, S. M. Asif, A. Fida, and R. M. Shubair, "A WLAN band-notched compact four element UWB MIMO antenna," *International Journal of RF and Microwave Computer-Aided Engineering*, Vol. 30, No. 9, e22282, 2020.
20. Puri, V. and H. S. Singh, "Design of an isolation improved MIMO antenna using metasurface based absorber for wireless applications," *Optik*, Vol. 259, 168963, 2022.
21. Parvathi, K. S. and S. R. Gupta, "Novel dual-band EBG structure to reduce mutual coupling of air gap based MIMO antenna for 5G application," *AEU — International Journal of Electronics and Communications*, Vol. 138, 153902, 2021.
22. Abbas, A., N. Hussain, M. A. Sufian, W. A. Awan, J. Jung, S. M. Lee, and N. Kim, "Highly selective multiple-notched UWB-MIMO antenna with low correlation using an innovative parasitic decoupling structure," *Engineering Science and Technology, an International Journal*, Vol. 43, 101440, 2023.

23. Luo, S., D. Wang, Y. Chen, E. Li, and C. Jiang, "A compact dual-port UWB-MIMO antenna with quadruple band-notched characteristics," *AEU — International Journal of Electronics and Communications*, Vol. 136, 153770, 2021.
24. Vasu Babu, K. and B. Anuradha, "Design of Wang shape neutralization line antenna to reduce the mutual coupling in MIMO antennas," *Analog. Integr. Circ. Sig. Process.*, Vol. 101, 67–76, 2019.
25. Suresh, A. C. and T. S. Reddy, "High isolation with fork-shaped stub in compact UWB-MIMO antenna using CMA," *2021 International Conference on Recent Trends on Electronics, Information, Communication & Technology (RTEICT)*, 505–511, 2021.
26. Suresh, A. C. and T. S. Reddy, "Design of corona shaped 2×2 UWB-MIMO antenna using characteristics mode analysis," *International Journal of Engineering Trends and Technology*, Vol. 70, No. 2, 260–269, 2022.
27. Singh, H. V. and S. Tripathi, "Compact UWB MIMO antenna with Fork-shaped stub with Vias Based Coupling Current Steering (VBCCS) to enhance isolation using CMA," *AEU — International Journal of Electronics and Communications*, Vol. 129, 153550, 2021.
28. Suresh, A. C. and T. S. Reddy, "A flower shaped miniaturized 4×4 MIMO antenna for UWB applications using characteristic mode analysis," *Progress In Electromagnetics Research C*, Vol. 119, 219–233, 2022.
29. Suresh, A. C., T. S. Reddy, B. T. P. Madhav, S. Das, S. Lavadiya, A. D. Algarni, and W. El-Shafai, "Investigations on stub-based UWB-MIMO antennas to enhance isolation using characteristic mode analysis," *Micromachines*, Vol. 13, No. 12, 2088, 2022.
30. Suresh, A. C., T. S. Reddy, B. T. P. Madhav, S. Alshathri, W. El-Shafai, S. Das, and V. Sorathiya, "A novel design of spike-shaped miniaturized 4×4 MIMO antenna for wireless UWB network applications using characteristic mode analysis," *Micromachines*, Vol. 14, No. 3, 612, 2023.
31. Gupta, S. K., R. Mark, K. Mandal, and S. Das, "Four element UWB MIMO antenna with improved isolation using resistance loaded stub for S, C, and X band applications," *Progress In Electromagnetics Research C*, Vol. 131, 73–87, 2023.
32. Jabire, A. H., S. Sani, S. Saminu, M. J. Adamu, and M. I. Hussein, "A crossed-polarized four port MIMO antenna for UWB communication," *Heliyon*, Vol. 9, No. 1, 2023.
33. Althuwayb, A. A., "Low-interacted multiple antenna systems based on metasurface-inspired isolation approach for MIMO applications," *Arabian Journal for Science and Engineering*, Vol. 47, No. 3, 2629–2638, 2022.
34. Desai, A., J. Kulkarni, M. M. Kamruzzaman, Š. Hubálovský, H. T. Hsu, and A. A. Ibrahim, "Interconnected CPW fed flexible 4-port MIMO antenna for UWB, X, and Ku band applications," *IEEE Access*, Vol. 10, 57641–57654, 2022.
35. Rekha, V. S. D., P. Pardhasaradhi, B. T. P. Madhav, and Y. U. Devi, "Dual band notched orthogonal 4-element MIMO antenna with isolation for UWB applications," *IEEE Access*, Vol. 8, 145871–145880, 2020.
36. Tiwari, R. N., P. Singh, B. K. Kanaujia, and K. Srivastava, "Neutralization technique based two and four port high isolation MIMO antennas for UWB communication," *AEU — International Journal of Electronics and Communications*, Vol. 110, 152828, 2019.
37. Faouri, Y., S. Ahmad, S. Naseer, K. Alhammami, N. Awad, A. Ghaffar, and M. I. Hussein, "Compact super wideband frequency diversity hexagonal shaped monopole antenna with switchable rejection band," *IEEE Access*, Vol. 10, 42321–42333, 2022.
38. Pannu, P. and D. K. Sharma, "Miniaturize four-port UWB-MIMO antenna with tri-notched band characteristics," *Microwave and Optical Technology Letters*, Vol. 63, No. 5, 1489–1498, 2021.
39. Khan, A. A., S. A. Naqvi, M. S. Khan, and B. Ijaz, "Quad port miniaturized MIMO antenna for UWB 11GHz and 13GHz frequency bands," *AEU — International Journal of Electronics and Communications*, Vol. 131, 153618, 2021.